Synergistic Mechanical and Chemical Activation of Kaolin Clays for Enhanced Reactivity in Limestone Calcined Clay Cement (LC^3)

Khuram Rashid[a,*], Nosheen Blouch[a,b], Miral Fatima[a], Mingzhong Zhang[c,*]

[a]Department of Architectural Engineering and Design, Faculty of Civil Engineering, University of Engineering and Technology, Lahore, Pakistan

[b]Department of Building and Architectural Engineering, Faculty of Engineering and Technology, Bahauddin Zakariya University, Multan, Pakistan.

[c]Department of Civil, Environmental and Geomatic Engineering, University College London, London, WC1E 6BT, UK

[*]Corresponding Authors. Email addresses: khuram_ae@uet.edu.pk (K. Rashid); mingzhong.zhang@ucl.ac.uk (M. Zhang)

Abstract

Limestone calcined clay cement (LC^3) produced from high-grade clays calcined at optimum temperatures demonstrates superior performance, while the utilisation of low-grade clays remains limited due to their reduced reactivity. To tackle this limitation, this study introduces an innovative multi-activation strategy that integrates calcination with simultaneous mechanical or chemical activation. Two clays with distinct kaolinite contents were subjected to this hybrid activation process, which were characterised using X-ray fluorescence (XRF), X-ray diffraction (XRD), thermogravimetric analysis (TGA), and modified Chapelle and R^3 tests. Subsequently, two grades of LC^3 mortar were prepared from the activated clays, and their hydration kinetics and strength development were evaluated up to 90 d. Results indicated that thermomechanical activation significantly enhanced the pozzolanic reactivity of both clays, leading to higher heat release and strength development, particularly for LG-based LC^3. Specifically, it showed a 35.5% increase in strength at 28 d compared to 7 d strength, while HG-based LC^3 exhibited a 46.5% increase. In contrast, thermochemical activation resulted in the formation of zeolitic phases that adversely affected reactivity, and thus there was reduction in bound water content and $Ca(OH)_2$ consumption for both clays, 15.3% and 17.9%, respectively as compared to thermal activation. Overall, thermomechanical activation demonstrated superior potential for improving the performance of low-grade clays, Finally, correlation matrices were established to link clay reactivity with strength development. Furthermore, a schematic model illustrating reactivity mechanisms under different activation strategies was proposed and verified through XRD and TGA analyses.

Keywords: Low-grade clays; Thermomechanical activation; Thermochemical activation; Pozzolanic reactivity; Hydration mechanism; Strength development

1. Introduction

Limestone calcined clay cement (LC^3) is an advanced ternary blended cement that allows up to 50% replacement of traditional clinker with a combination of calcined clay and limestone [1]. LC^3 generally exhibits a refined microstructure with superior mechanical properties and durability compared to conventional supplementary cementitious materials (SCMs), particularly at high cement replacement levels [2, 3]. The performance of LC^3 largely depends on the type and reactivity of the clay used [4]. While high-grade kaolinite clays (>40% kaolinite) are preferred for higher clinker replacement (LC^3-50) [5], low-grade clays (<20% kaolinite) can also be utilized for lower replacement levels (LC^3-30) [6]. To enhance the reactivity of low-grade clays, activation techniques beyond thermal calcination must be explored.

Mechanochemical activation treatment has proven to be quite useful for activating clay minerals that are difficult to activate by thermal treatments [7, 8]. The process represents a straightforward approach accomplished through extensive milling. Thus, resulting to improve clay reactivity by reducing particle size, increasing surface area, and inducing structural disorder, while requiring relatively low energy [7, 8]. Chemical activation, through acid or alkaline treatments [9, 10], can further amorphize clay minerals and enhance their pozzolanic potential, though careful optimization is required to avoid undesired mineralogical changes [11-13]. In the context of LC^3 systems, recent studies suggest that mechanochemical activation can enhance the reactivity of low-grade clays and improve their contribution to hydration and strength development, although systematic understanding and optimisation are still evolving.

Similarly, chemical activation methods can also be used to amorphize the layer structure of clay minerals through partial dissolution. This technique has been widely employed through both acid [11] and alkaline treatments [12, 13], which can improve the surface and catalytic properties of smectitic clays [14], and amorphize kaolins [15]. Both montmorillonite and illite can be highly amorphized with a treatment optimised for concentration and duration of exposure [16, 17]. However, chemical activation may lead to unintended changes in mineral composition, e.g., chemical reaction forming zeolite or an increase in the Si:Al ratio, which may impact the pozzolanic potential. It is therefore advisable to optimise the process parameters according to the clay mineral's composition to get the desired pozzolanic potential. In LC^3 systems, chemical activation may also offer alternative strategies to improve clay reactivity beyond conventional calcination.

It is vital to investigate the pozzolanic reactivity of clay after activation for assessing its suitability as an SCM [18]. Both direct and indirect methods are available to assess the pozzolanic activity of calcined clays [19]. The author recent paper summarises the methods of reactivity of clay for developing LC^3 [4]. Conventional direct test methods such as the modified Chappelle and Frattini tests can serve as quick assessment tools for pozzolanic behaviour directly through calcium hydroxide

consumption. They are rapid, quantitative and correlate well with compressive strength [20]. However, it is worth noting that the interpretation of the chemical process involving lime fixation by pozzolana is based on binary mix formulations that may not completely mimic the performance of SCM in complex systems like LC^3 [21]. Avet et al. [22] presented a non-conventional, rapid, relevant, and reliable (R^3) direct testing approach for estimating the reactivity of calcined-clay. The R^3 recipe enables some assessment of more complex systems by using calcined clay, Portlandite, and limestone-based pastes, in which sulphate and alkali levels are adjusted to mimic the reaction environment of hydrated blended cements. RILEM TC 267-TRM assessed the effectiveness of both conventional and novel reactivity test methods [23], and demonstrated that R^3 test, using either isothermal calorimetry or bound water determination, shows the strongest correlation with mortar compressive strength [24].

Although LC^3 has been extensively studied in terms of hydration mechanisms, microstructural evolution, and mechanical properties development, the summary of main themes of the available review articles have been prepared and presented in another review article [4]. Most studies focus on high-grade clays activated thermally, limiting broader industrial adoption. Alternative activation strategies; mechanochemical, chemical, or combined, offer potential to enhance the performance of low-grade clays sustainably. This study systematically evaluates these activation methods on two clays of differing reactivity, assessing their influence on LC^3 performance, including compressive strength evolution and hydration behaviour. The aim is to provide insights into sustainable approaches for LC^3 production with low-grade clays.

This study aims to explore and monitor the pozzolanic potential of two clays activated through (i) calcination at different temperatures, (ii) extensive milling, (iii) chemical treatment through alkaline activation, and (iv) a combination of these treatments, designed to ensure a sustainable low-carbon application of the emerging LC^3 cementitious system. The two chosen clays, namely high-grade and low-grade kaolins with distinct reactivity profiles, facilitated the observation of varied responses to the applied activation methods. After activation, the performance assessment of LC^3 was carried out considering both short- and mid-term properties of LC^3 blends including compressive strength evolution and hydration mechanisms. Overall, this study intends to provide a comprehensive understanding of the potential of alternative methods to activate the low-grade clays for use in LC^3, which may reduce the impact of high-energy thermal activation.

2. Experimental program

2.1 Raw materials

LC^3 was manufactured with constituents including ordinary Portland cement (OPC), limestone, and clay. OPC conforming to ASTM Type-I and medium-grade limestone were used in this study. The chemical compositions of OPC and limestone determined using X-ray fluorescence (XRF) are

provided in Table 1. Two clays were used to develop LC^3: both clays were collected from the vicinity of cement plants in Pakistan, which were pulverized in fine powder using a jaw crusher to break down larger materials and then passing through a Denver McCool ball mill (USA) at 150 rpm for 5 min to reduce the particle size. Although only two clays were studied here, they were selected based on a previous broader investigation of 19 clay samples by the authors. The chosen high-grade (HG) and low-grade (LG) clays represent the extremes of kaolinite content and reactivity, enabling a focused and representative evaluation of activation strategies in LC^3 systems. **Fig. 1** shows the particle size distribution of different materials. D_{50} of OPC and limestone is 21.0 and 15.3 µm, respectively. D_{50} of Clay 1 is 4.5 µm and that of Clay 2 is 11µm. The pulverized clays were used for XRF analysis, and their composition is provided in **Table 1**.

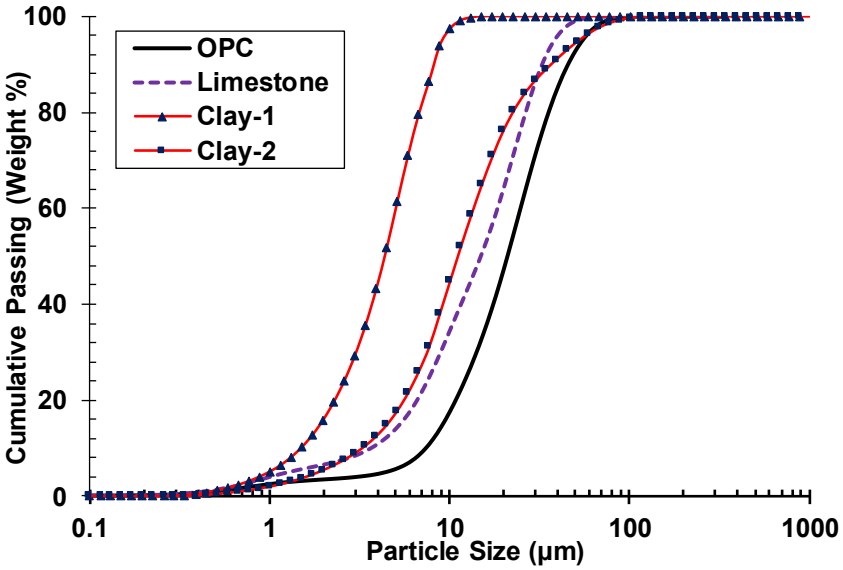

Fig. 1. Particle size distribution of binders used in this study.

Table 1 Chemical compositions (wt.%) of binders used in this study.

Binder	SiO_2	Al_2O_3	Fe_2O_3	CaO	MgO	K_2O	Na_2O	SO_3	Cl
OPC	19.4	4.8	3.5	60.9	2.6	2.7	0.3	0.8	0.0
Limestone	19.3	5.4	2.1	42.5	1.0	0.8	0.4	0.2	0.0
Clay 1 (HG)	58.7	28.8	3.5	2.3	0.2	0.3	0.1	0.2	0.0
Clay 2 (LG)	66.4	19.6	7.0	4.7	1.7	1.5	1.4	0.1	0.7

The weight loss at 200 ($Wt_{200°C}$), 400 ($Wt_{400°C}$), and 600 ($Wt_{600°C}$)° were used to quantify the kaolinite content in each clay following Eq. (1) [25] and using a simple oven and balance. $M_{kaolinite}$ and M_{water} in Eq. (1) are molecular weight and their values are 258g/mol and 18g/mol, respectively. Wt_i is the initial weight of uncalcined clay. The kaolinite content for both clays is 55% and 25%. Based on the kaolinite content, the clays are designated as high-grade kaolinite clay "HG" and low-grade kaolinite clay "LG" in this study.

$$Wt\%_{Kaolinite} = \frac{Wt_{400°C} - Wt_{600°C}}{Wt_{200°C} - Wt_i} \times \frac{M_{Kaolinite}}{2M_{Water}} \times 100 \quad (1)$$

X-ray diffraction analysis (XRD) was conducted to determine the mineralogical composition of clays, which is presented in **Fig. 2**. The presence of kaolinite (K) and quartz (Q) was evident in HG, whereas in LG, kaolinite (K), quartz (Q), calcite (C) and illite (I) can be identified.

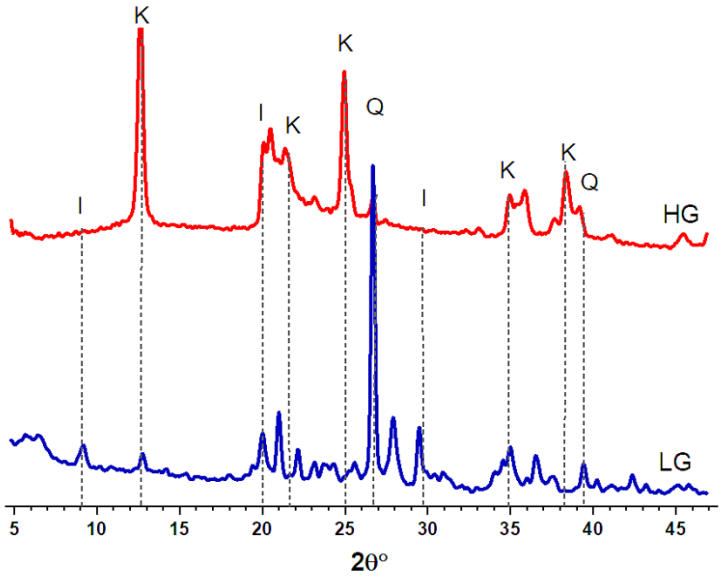

Fig. 2. XRD patterns of raw clays.

2.2 Activation of clay

For the thermal activation treatment, denoted with the postscript "T" (**Fig. 3**), calcination was conducted at either 750 °C (HG-T) or to 900 °C (LG-T) for 1 h at the heating rate of 30 °C/min in a laboratory Muffle furnace (Ney VULCAN D-550). Small variations in the colour of the clays can also be observed due to the calcination. TGA was used to determine the optimum temperature for pozzolanic reactivity [26, 27] and amorphization or disappearance of clay mineral-related reflections were observed via XRD analysis.

An additional mechanical activation was applied to a portion of the materials processed as described above, except that the calcination temperatures were reduced by 50 °C (i.e., 700 °C for HG-T and 850 °C for LG-T). Both clays were processed using a laboratory ball mill with a motor and disk speed of 1800 rpm and 250 rpm, respectively, to further reduce particle size and potentially increase the reactivity. These are denoted with the postscript "TM" (HG-TM, LG-TM) in **Fig. 3**.

A third technique coupled an alkaline chemical treatment, denoted with the postscript "TC" (**Fig. 3**). For chemical activation, 5 molar concentrations of NaOH were mixed with HG-T and LG-T at a solvent to clay ratio of 5 mL/g and clay soaked for 3.5 h, agitated and then dried in oven at 150 °C, followed by centrifugation (3500 rpm for 2 min) to separate the solids. The solid fractions were then washed with de-ionized water at 10 – 15 L/kg (L/S ratio) using a vacuum filtering system until wastewater with a near-neutral pH of 7 – 8 was achieved. The resulting filtrate (HG-TC and LG-TC) was then dried at 100 °C to a constant weight before further use.

2.3 Mix proportions and specimen preparation of LC^3 mortar

LC^3-based mortar was prepared in this study in two series. For each clay, three activation techniques were employed, resulting in a total of six activated clays. In the first series, six different mortar specimens were prepared using the T, TM, and TC activated HG and LC clays as illustrated in **Fig. 3**, where "M" for "mortar", HG or LG for clay type, and T, TM or TC for activation treatment were applied. Lawrencepur sand from Lawrencepur Punjab, Pakistan with a fineness modulus of 2.7 was used as the aggregate in the mortar mixes. Mortars were prepared as per ASTM C109 [28] with cement:sand ratio of 1:2.75 and water-to-cement ratio of 0.48. Cement consists of ternary constituents, i.e., OPC, limestone, and calcined clay. For the initial trial, 30% OPC was replaced with calcined clay and limestone, maintaining their proportion at 2:1 (LC^3-30). The 50 mm cube specimens were prepared and cured in ambient conditions until testing.

A second series of mortar (Series-2) was prepared using the best performing calcined clay out of the three activated techniques in the first series and LC^3-50 mortar was prepared (**Fig. 3**), where 50% cement was replaced with a similar 2:1 for calcined clay-to-limestone ratio.

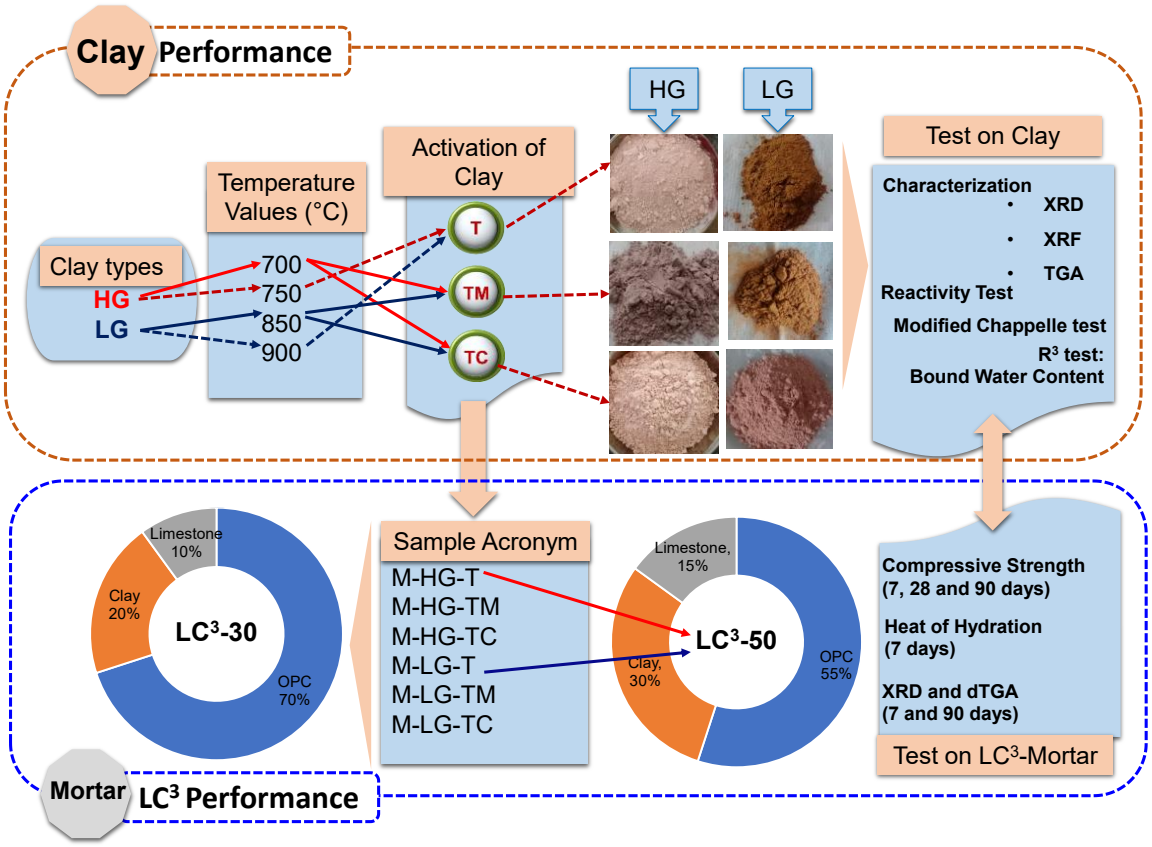

Fig. 3. Activation regimes of the used clays and summary of tests performed to assess the activation index in this study.

2.4 Test methods

The activated clays were characterised, and their reactivity was assessed. A summary of the treatment of clays and tests performed is given in **Fig. 3**. The detailed procedure of the tests and the instrument used for testing are explained below.

2.4.1 Characterisation of original and activated clays

XRF analysis was conducted on pressed powdered samples to examine the changes in chemical composition caused by activation treatments using a PANalytical Smart Zetium X-XRF spectrometer. Around 10g of treated clay was mixed with 3 wax tablets and homogenised for 2 min. The mixture was then pressed under 150 kN force to make pellets. Pellets were preconditioned before the analysis. The mineralogical composition of the activated clays was analysed by XRD using a BTX III Benchtop XRD Analyzer. The 75-micron sample was carefully backloaded and the analysis was carried out with Cu kα radiations using 30 mA current and 30 kV voltage, respectively. The scanning range was set at 5 – 50 °2θ with a step size of 0.025 °2θ.

The thermal behaviour of both untreated and treated clays was examined by TGA/DTG analysis. TGA was performed using a LINSEIS STA PT 1600 (TG-DSC) by heating the samples (approximately 36 mg, size < 425 µm) in an alumina crucible at a rate of 10 °C/min, starting from 50 °C up to a maximum temperature of 950 °C using N_2 as a purge gas.

2.4.2 Modified Chapelle test

The reactivity of clays after activation (T, TM, TC) was assessed following the modified Chapelle test procedure (French standard NF P18-513) [23]. For evaluating reactivity, 1 g of calcined clay was mixed with 2 g of hydrated lime (CH) and 250 ml of distilled water. For comparison, blank samples without calcined clay were also tested. The mixture was then heated at 90 °C for 16 h under a reflux condenser to prevent water loss. Following cooling to 20 °C, a solution of 60 g of sucrose in 250 ml of deionized water was added to complex calcium ions and dissolve unreacted portlandite. After filtration, the liquid was titrated with 0.1 M HCl using phenolphthalein as a pH indicator. The amount of bound portlandite was calculated using Eq. (2), where V_1 and V_2 represent the volumes of HCl solution added for the blank and calcined clay samples, respectively.

$$\text{mg CH/g of activated clay} = 2\frac{V_1 - V_2}{V_1}.\frac{74}{56}.1000 \quad (2)$$

2.4.3 R^3 test: bound water content

The R^3 bound water method was used to measure the reactivity of the activated clays. The mixture used to measure the bound water content included $Ca(OH)_2$, activated clay, calcite ($CaCO_3$), alkali (KOH), and sulfate (K_2SO_4) according to the mix proportions presented in **Table 2**. The RILEM TC 267 TRM, Phase 2 Report [29] served as the basis for the formulation of the mixture for this test. After mixing the constituents by hand for 5 min, the fresh paste was cured at 40 °C in sealed plastic

containers for 7 d. The paste was crushed after being taken out of the oven, and ≈10 g of the < 2 mm particles (accurately weighed) was then placed in a crucible.

Table 2 Mix proportion for calculating bound water content: R^3 paste.

Constituent	Clay	Portlandite	Calcite	KOH	K_2SO_4	Deionized water
Mass (g)	11.11	33.33	5.56	0.24	1.2	60

The powdered paste specimen was then heated in an oven at 105 °C for 2 h. The dried sample was then heated in a lab oven for 2 h at 350 °C and was consequently cooled in a desiccator for 1 h without a vacuum over silica gel. The weight of the sample was measured after each heating or drying step. Care was taken while transferring sample to and from the desiccator and oven for weight measurement to avoid exposure to the atmosphere for too long. The weight loss between drying and 350 °C, normalised by the weight of the dried sample, was used to calculate the amount of bound water from Eq. (3). Weight loss corresponds to the dehydration of the hydration products. Bound water was used as a direct indicator to determine the reactivity of clays.

$$Bound\ water\ (\%) = \frac{W_0 - W_{(350)}}{W_0 - W_c} \times\ 100 \qquad (3)$$

where W_c denotes the mass of empty crucible, W_o represents the mass of the crucible plus dried paste, and W_{350} stands for the weight of crucible plus the paste after drying at 350 °C.

2.4.4 Characterisation of LC^3 mortar

The compressive strength of LC^3 mortar was measured at 7, 28 and 90 d as per ASTM C109 [28]. Three specimens for each mixture were tested, and the average value was taken as compressive strength. Post-fracture, crushed particles were processed to conduct detailed XRD and TGA analyses, which enabled a comprehensive exploration of material behaviour and composition, emphasising the profound implications of reactivity on performance. The heat of hydration of LC^3 and OPC was measured over 7 d using an isothermal conduction calorimeter (ICC) as per ASTM C1702 [30]. The entire testing methodology adopted in this study to analyse the performance of activated clays to the LC^3 mortars is displayed in **Fig. 3**.

3. Experimental results

3.1 Characteristics of activated clays

3.1.1 Chemical composition

The activated clays, after all three regimes (T, TM, and TC), were examined for oxides composition, and XRF analysis of raw as well as activated clays is presented in **Table 3**. Slight changes can be observed when oxides of raw and activated clays were compared. With respect to T treatment, changes can be ascribed to the effective removal of predominantly water (and perhaps carbon dioxide (CO_2) on oxidation of minor organic matter or breakdown of minor carbonates) during heating. The percentage of silica (SiO_2) reduced in both clays while the alumina (Al_2O_3) increased in

HG and showed a slight drop in LG. During thermal activation, the coordination of Al shifts from VI-fold to V- and IV-fold due to dehydroxylation induced changes in the clay structure [15, 31, 32]. LOI was also noted to significantly reduce. These findings were well aligned with literature [33, 34].

Oxides of TM activated clays were very similar to T activated clays as the dehydroxylation already occurred in the thermal stage, while further mechanical processing was intended to enhance the structural disorder, and to increase fineness and surface area of the clay. XRF analysis revealed significant changes in the chemical composition of the clay samples after the TC process, including a significant increase in Na_2O content, which indicated the incorporation of sodium ions (Na^+) into the clay structure [35]. Na_2O present in trace amounts in raw clays increased to significant levels in both clays after TC. The silica content was considerably decreased in both clays (26% for HG and 13% for LG), possibly due to chemical reaction of silica with basic solution.

Table 3 Chemical compositions (wt.%) of raw and activated clays.

Clay	Activation	SiO_2	Al_2O_3	Fe_2O_3	CaO	MgO	K_2O	Na_2O	Cl	LOI
HG	---	58.7	28.8	3.5	2.3	0.2	0.3	0.1	0.0	12.2
	T	53.2	34.3	3.4	2.7	0.0	0.0	0.0	0.0	3.0
	TM	54.2	33.0	3.4	2.7	0.0	0.0	0.0	0.0	2.4
	TC	43.1	31.0	2.2	2.0	0.1	0.1	12.0	0.0	13.1
LG	---	57.75.4	19.6	7.0	4.7	1.7	1.5	1.4	0.7	10.3
	T	64.1	18.6	7.1	4.6	1.8	1.6	1.6	0.2	0.5
	TM	63.8	18.1	7.1	5.0	1.8	1.5	1.6	0.1	0.4
	TC	57.5	18.6	6.8	4.6	1.8	1.1	6.6	0.3	6.2

3.1.2 Mineralogical composition

Initially, the clays were calcined at temperatures ranging from 700 to 900 °C to achieve optimum amorphization; the diffractograms of raw and calcined clays are compared in **Fig. 4**. For HG calcined at 700 °C, a few residual kaolinite peaks were observed, showing incomplete dehydroxylation. However, the complete disappearance of most of the kaolinite peaks at 750 °C indicated complete kaolin-metakaolin transformation. The presence of a raised background within 20 to 40° 2θ is typical for amorphization of kaolin into metakaolin [36]. Quartz peaks remained mostly unchanged after calcination because calcination at given temperatures does not alter quartz structure [37]. The XRD patterns indicated substantial structural changes with increasing calcination temperature from 850 °C to 900 °C; the intensity of illite reflections dropped with increasing temperature confirming increased dihydroxylation, especially the characteristic illite reflection at around 9° 2θ disappeared after 900 °C (**Fig. 4**). Even after calcination at 900 °C, not all the illite peaks were completely removed, indicating that layered structure of illite remained largely intact even after dehydroxylation [36]. The XRF result indicated a greater percentage of silica in LG (being dominant with 2:1 layered silicates

or quartz impurities), which was verified from significantly greater reflections of quartz in LG compared to HG.

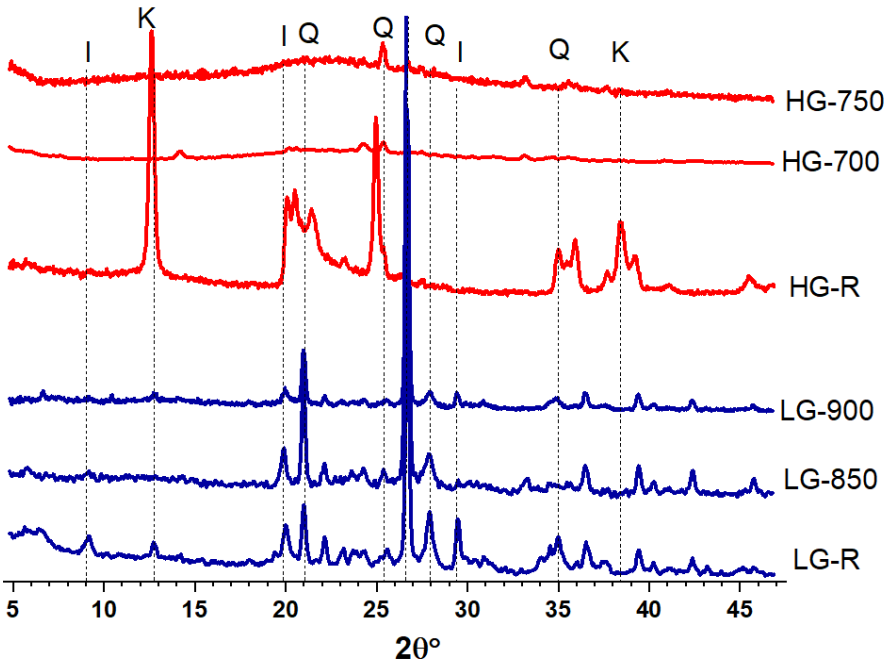

Fig. 4. XRD patterns of raw and calcined clays at different temperatures (I: Illite; K: Kaolinite; Q: Quartz).

Partially calcined clays at 700 °C (HG) and 850 °C (LG) underwent additional grinding/milling to achieve increased amorphization through TM activation. **Fig. 5** displays the XRD patterns of clays activated with different methods in comparison with that of raw clays. XRD of HG (TM) showed the disappearance of residual and low-intensity reflections of kaolinite after milling. The disappearance of kaolinite peaks at 12.4, 18.4, and 24 °2θ suggested the breaking of the bonds and structural disorder between kaolinite layers [37]. The intensity of characteristic quartz peak at 26.7° 2θ decreased in HG with observed peak broadness, implying grinding and collapse of quartz particles. Whereas the quartz peak intensity in LG increased along with the reduced illite/kaolinite intensities, possibly due to the further dehydroxylation and release of silica from the illite structure due to rigorous grinding. The effectiveness of mechanical activation varied with clay type, which was reported to be more beneficial for illite or smectite clay [38]. Apart from the structural changes observed in XRD, the rise in specific surface area and drop in particle size achieved through mechanical activation can enhance the reactivity and performance of the clay minerals [39].

Structural modification induced by partial calcination of kaolinite at 700 °C led to conversion into zeolite upon exposure to 5 M NaOH solution, as confirmed by various reflections in the XRD patterns attributed to zeolite of HG-TC (**Fig. 5**). The intensity and shapes of these peaks reflected the degree of crystallinity of zeolite phases formed [40, 41]. However, altering the calcination temperature, concentration and/or duration of NaOH exposure could favour metakaolin formation and impede the

development of zeolite-like minerals, which is a further research interest and work is currently undergoing in that direction. XRD patterns of LG (TC) resembled that of LG (TM) except for the emergence of few zeolite peaks (14.9, 25.9° 2θ [35]) and minor changes in quartz peaks. The intensity of illite/kaolinite peaks reduced as well. The phase evolution observed through XRD is fully consistent with the underlying activation mechanisms. In thermally activated clays (T), the disappearance of kaolinite reflects transformation into metakaolin, an amorphous aluminosilicate with high internal disorder and abundant reactive Al–OH vacancies [36]. TM activation introduces an additional mechanochemical effect: milling imposes high local shear and impact forces that generate structural defects, break lamellar stacks, and increase the proportion of amorphous phase. These defects act as high-energy reaction sites that enhance pozzolanic reactivity even when calcination temperature is reduced by 50 °C [37, 39]. Conversely, TC activation induces partial dissolution of the aluminosilicate framework in alkaline solution, followed by reprecipitation of sodium–aluminosilicate hydrates (zeolitic precursors) [40, 41]. This explains the emergence of broad low-intensity humps and the suppression of the typical metakaolin halo. While these phases reduce early reactivity due to structural reorganization, they provide long-term ion-exchange and alkali-binding potential, influencing later-age hydration behaviour.

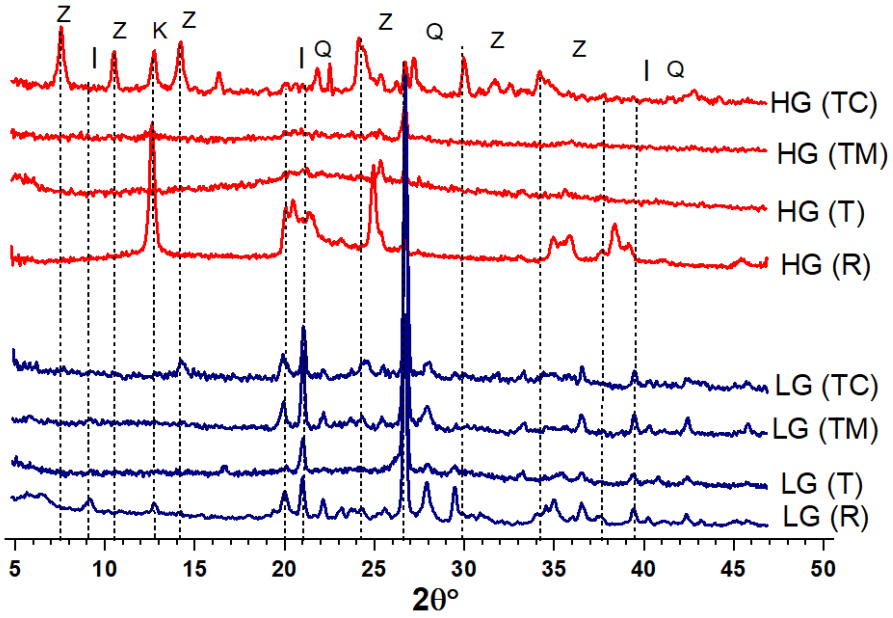

Fig. 5. XRD patterns of raw clays and clays activated with different methods (I: Illite; K: Kaolinite; Q: Quartz; Z: Zeolite).

3.1.3 Thermal behaviour

Fig. 6(a) illustrates TGA of both raw clays along with the differential of TGA (dTGA), indicating that the weight loss in HG was 12.5%, whereas the weight loss in LG was 6% only. The dTGA curve of the LG clay exhibited two distinct weight loss events. The first weight loss event within 200 – 250 °C can be ascribed to dehydration of surface absorbed water possibly due to mica/illite/smectite [42],

decomposition of some organic impurities, and/or some partial dehydroxylation indicating a phase transition or start of decomposition process. HG exhibited negligible weight loss in this region, while LG showed about 4% weight loss. The second peak (within 500 – 700 °C in case of HG and 450 – 600 °C in the case of the LG) denoted the dehydroxylation of kaolinite, as per the findings of Refs. [36, 43]. The weight loss related to second peak was about 12% for HG and around 2% for LG confirming the greater kaolinite content in HG.

Efficient and complete dehydroxylation was achieved for T and TM-activated clays after processing as indicated by the relative lack of any dTGA profile (**Fig. 6**(b)). The dTGA curves of TC-activated clays yielded a stable weight loss up to 400 °C, indicating the conversion of kaolinite/illite layered structure into zeolite [44], with the weight change likely associated with water loss from zeolite phases. The TGA weight loss in HG-TC (13.10%) was almost double that of LG-TC (6.08%), which appeared to correlate with XRF analyses: Na_2O in HG-TC was almost double that of LG-TC. The observed trends can be mechanistically explained by the mineralogical differences between HG and LG. The larger mass-loss associated with HG is consistent with its higher kaolinite content, since dehydroxylation of kaolinite ($Al_2Si_2O_5(OH)_4 \rightarrow Al_2Si_2O_7 + 2H_2O$) proceeds sharply within a narrow temperature window and releases structurally bound hydroxyl groups [36, 43]. In contrast, LG exhibits a broader dehydroxylation hump due to the presence of mixed-layer illite–smectite phases, whose OH groups are removed progressively over a wider temperature interval [42]. The negligible shift in mass-loss behaviour for TM and TC treatments indicates that neither mechanical nor mild alkaline processing alters the primary thermal decomposition pathways of the clay minerals. However, TC-treated clays show slightly smoother dehydroxylation shoulders, attributable to partial dissolution and reprecipitation of aluminosilicate species, which disrupt long-range order and broaden the thermal response. The stable weight loss of TC upto 400 °C is attributed to the formation of zeolite [44]. These mechanistic differences in dehydroxylation behaviour directly underpin the reactivity variations observed in subsequent pozzolanic and hydration tests. Overall, dTGA observation agreed with the results of XRF (Section 3.1.1) and XRD (Section 3.1.2).

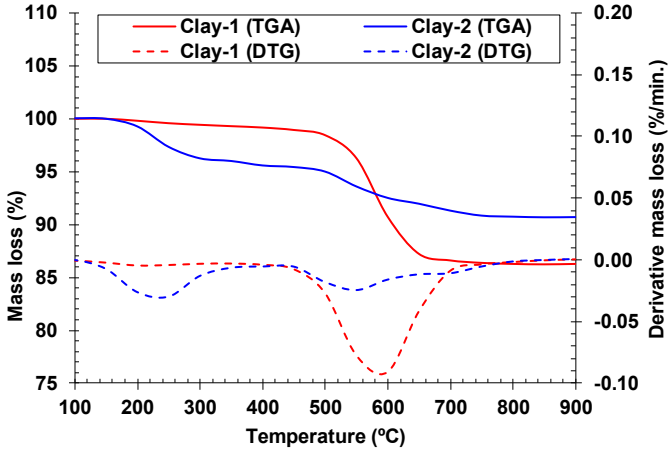

(a)

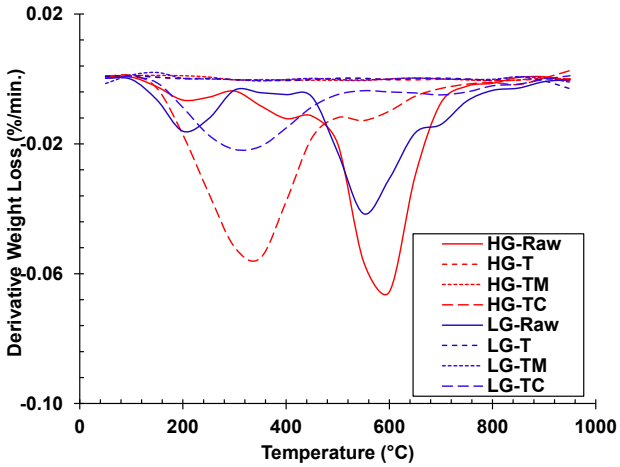

(b)

Fig. 6. Thermal analysis of raw clays (a) and dTGA of raw and activated clays (b).

3.1.4 Reactivity assessed by the modified Chappelle test

Fig. 7 presents the results of the modified Chapelle test, where notable differences in the reactivity of activated HG and LG can be observed. The Portlandite consumption in the blank sample was 7135 mg/g of CaO. HG presented greater Portlandite consumption than LG in all activation scenarios. For instance, after TM activation, HG exhibited greater reactivity with a Portlandite consumption of 1174 mg/g of clay compared to LG, which showed a reactivity value of 880 mg per gram of clay. These results are in complete compliance with XRF (**Table 3**) and XRD (**Fig. 6**) findings whereby higher and lower amorphous (reactive mass) were recorded for HG and LG, respectively. Avet et al. [22] also reported similar results and found 500, 1100, and 1500 mg $Ca(OH)_2$/g of calcined-clay for the kaolinite clays containing 35%, 50.8%, and 95% calcined kaolinite content, respectively. Considering the activation methods, the Portlandite consumption was highest for T-activated clays and was lowest for TC-activated clays. The Portlandite consumption results are consistent with the kaolinite content, chemical composition, XRD patterns, and structural modifications induced by the activation processes.

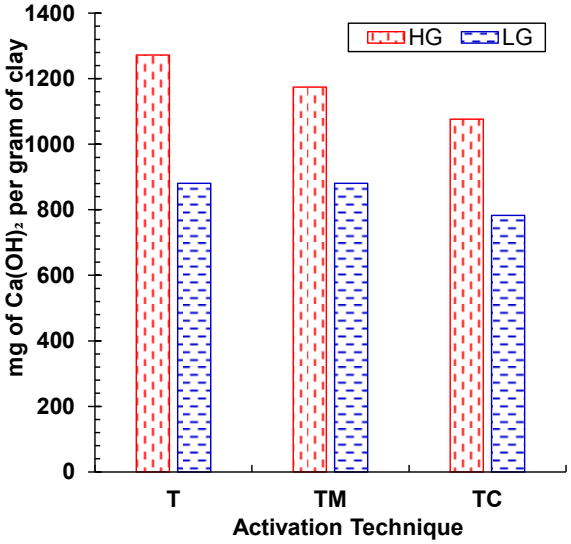

Fig. 7. Portlandite consumption of all the clays.

3.1.5 R^3 bound water content

Fig. 8 displays the bound water content in calcined clay-limestone blends cured for 7 d, measured by the R^3 test. TM activation was found to be most effective for HG, indicating the greatest bound water content in both clays and among different activation techniques. The peak value of more than 8% was recorded for HG, suggesting a higher reactivity due to higher kaolinite content. The bound water of T activated clay was only marginally lower than the TM-activated HG possibly due to the increased fineness and amorphization in TM processing [45, 46]. In addition, the TM activation might have also improved the reactivity of the impurities (e.g., quartz) by inducing structural disorder and amorphization [47]. The reduced reactivity of TC-activated clays can be attributed to the structural modification due to zeolite formation as indicated by XRD.

A correlation was established between the reactivity test results from both test methods i.e., modified Chappelle test and bound water content and R^2 value of 0.99 was obtained, indicating the accuracy and correspondence of the test results (**Fig. 9**).

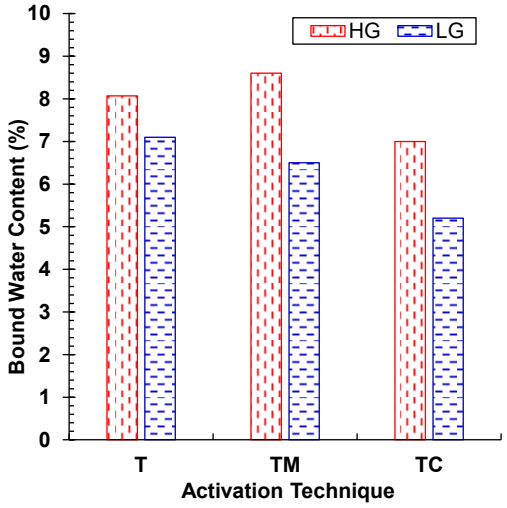

Fig. 8. Bound water content of all samples.

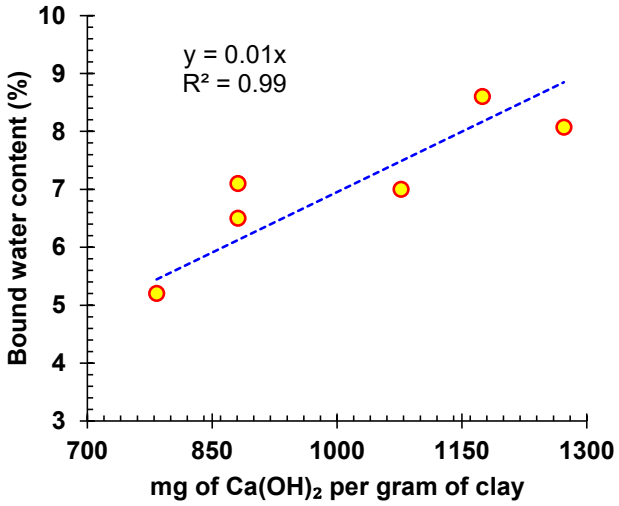

Fig. 9. Correlation of Portlandite consumption and bound water content.

3.2 Role of activated clays in LC^3

3.2.1 Hydration kinetics

Fig. 10 presents a detailed comparison of the cumulative heat generated during the hydration process of OPC and various LC^3 mixes. M-HG-T exhibited the greatest heat of hydration among all LC^3 samples can be ascribed to the increased reaction efficiency of cement because of the filler effect and the enhanced phase formation due to pozzolanic effect of clays and limestone. The blends containing clays with greater reactivity exhibited greater hydration heat [48], however, after an initial surge over the first three days, the heat generation rate started to drop gradually as expected [49].

T and TM-activated clay-based LC^3 blends exhibited greater heat of hydration compared to TC throughout the 7 d observation period. The M-HG-T blend exhibited a pronounced exothermic nature,

which distinguished it from M-HG-TM and M-HG-TC. However, LC^3-LG-T and TM showed comparable heat release patterns, indicating the effectiveness of mechanical activation for low-grade clays. On the other hand, chemically activated clay-based LC^3 blends exhibited the lowest heat of hydration, mainly ascribed to their lower reactivity.

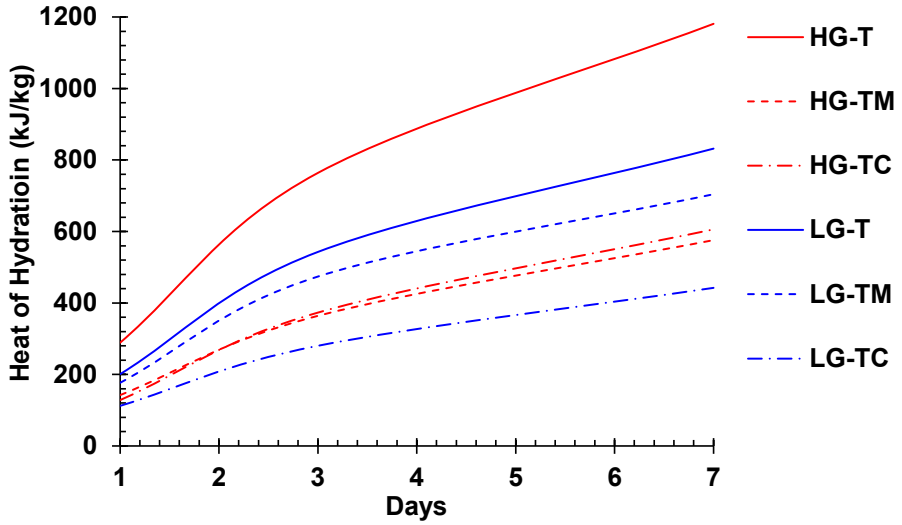

Fig. 10. Cumulative heat release of HG and LG based LC^3 blends up to 7 d.

3.2.2 Phase assemblage

Fig. 11 illustrates the XRD spectra for OPC and LC^3 samples cured for 7 and 90 d. At 7 d (**Fig. 11**(a)), both OPC and LC3 mixes exhibited ettringite reflections at ~9.1°, 15.9°, and 23.0° 2θ, along with mono-carboaluminate (Mc), portlandite (CH), calcite, and quartz reflections [42, 50]. CH reflections were higher in OPC, while significantly reduced in LC^3 due to the combined dilution and pozzolanic reactions [42, 50]. Interestingly, calcite reflections were comparable between OPC and LC^3 despite higher limestone content in LC^3, indicating limestone consumption in forming low-density carbo-aluminate phases.

HG-based clay mixes (M-HG) showed stronger ettringite and Mc reflections compared to LG-based mixes (M-LG), consistent with higher reactive alumina content and pozzolanic reactivity. TM and TC further enhanced the intensity of low-density phases in HG-based LC^3. Increasing clay content from LC^3-30 to LC^3-50 also promoted these phases, although overall dilution reduced 28-d compressive strength. At 90 d (**Fig. 11**(b)), ettringite reflections decreased while Mc reflections slightly increased in HG-based LC^3, reflecting ettringite transformation, pozzolanic reaction continuation, and possible monosulfate (Ms) formation due to sulphate depletion [51, 52]. LC^3-TC showed slightly lower peak intensities, suggesting reduced hydration reactions.

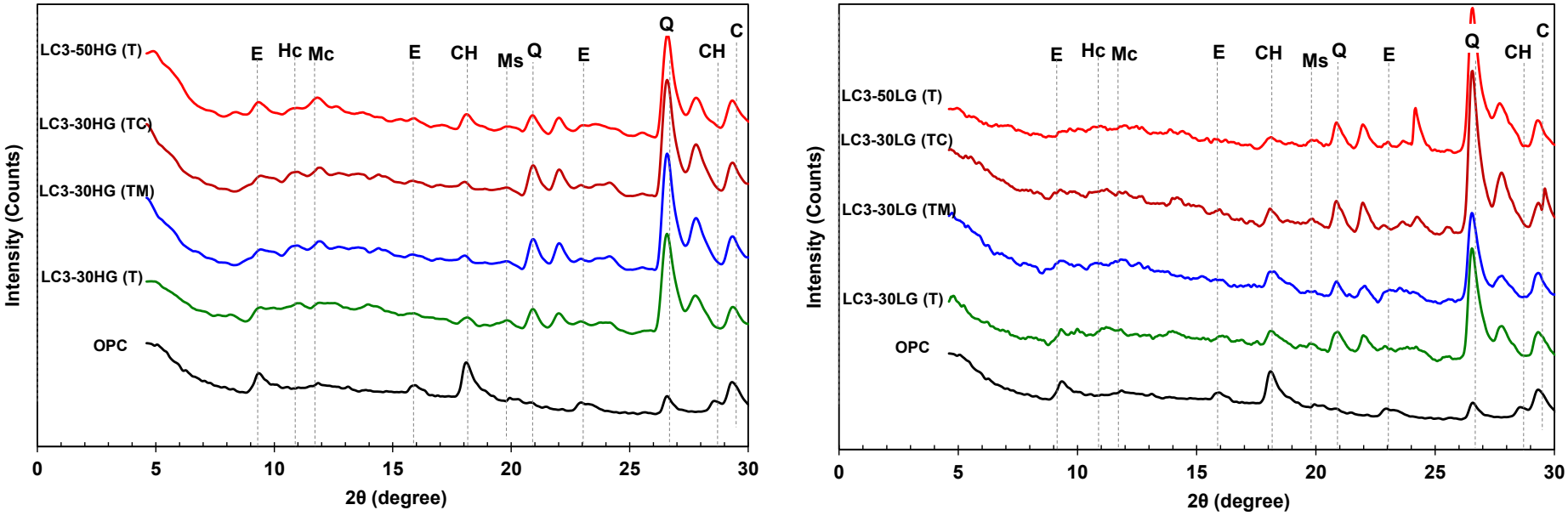
LC3-50HG (T)
LC3-30HG (TC)
LC3-30HG (TM)
LC3-30HG (T)
OPC
E
Hc
Mc
E
CH
Ms
Q
E
Q
CH
C
Intensity (Counts)
2θ (degree)
LC3-50LG (T)
LC3-30LG (TC)
LC3-30LG (TM)
LC3-30LG (T)
OPC
E
Hc
Mc
E
CH
Ms
Q
E
Q
CH
C
Intensity (Counts)
2θ (degree)

(a)

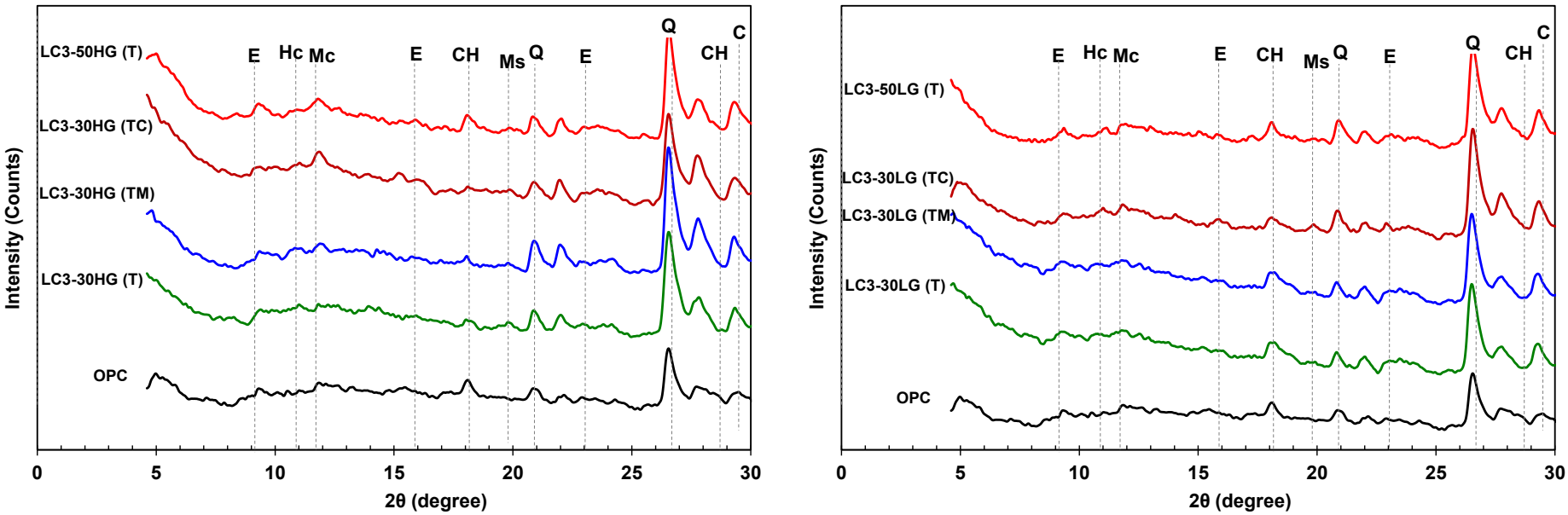

(b)

Fig. 11. XRD of OPC and hydrated LC^3 paste at: (a) 7 days and (b) 90 days. Note: Ettringite (E.); Portlandite (CH); Monocarboaluminate (Mc); Hemicarboaluminates (Hc); Monosulphate (Ms); Quartz (Q); Calcium carbonate (C).

Thermal analysis (**Fig. 12**) confirmed these observations. Endothermic peaks corresponding to ettringite, Mc, Ms, CH, and $CaCO_3$ were consistent with XRD results. T and TM activated clay-based LC^3 exhibited more intense peaks for ettringite, Mc, and Ms, attributed to enhanced clay reactivity and higher aluminate content. Chemically activated LC^3 showed lower AFt and AFm formation, but increased weight loss over 7–90 d indicated ongoing phase development, aligning with compressive strength trends. CH peaks decreased due to pozzolanic reactions, while $CaCO_3$-related weight loss increased in chemically activated clays, likely due to zeolite-mediated CO_2 adsorption forming soluble calcium bicarbonates.

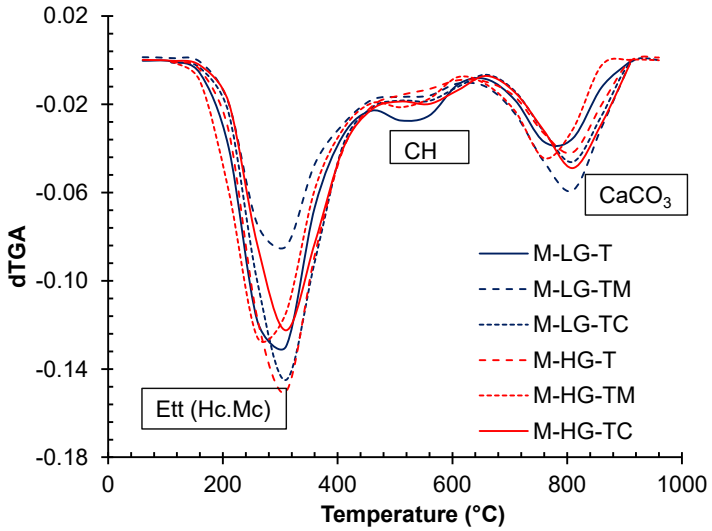

(a)

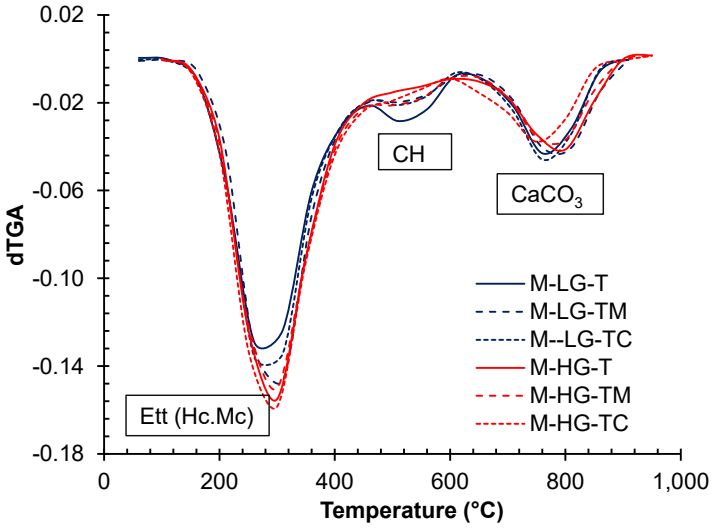

(b)

Fig. 12. TGA of hydrated cement paste at (a) 7 d and (b) 90 d.

These hydration signatures reflect distinct mechanistic contributions of the activation methods. Metakaolin-rich T-activated clays rapidly consume portlandite through pozzolanic reactions, forming C-A-S-H gels with higher Al incorporation, which explains the stronger reduction in CH peaks at 28 and 90 days [48]. TM activation accelerates this mechanism further: the defect-rich and finer particles

dissolve more readily in the alkaline pore solution, increasing the availability of reactive silica and alumina and promoting denser C-A-S-H and carboaluminate assemblages [45, 46]. In contrast, TC activation initially suppresses reactivity due to the presence of emergent zeolitic structures that dissolve more slowly [35]. However, the same phases participate in ion-exchange processes at later ages, enabling continued but delayed CH consumption and AFm-type phase stabilization [53, 54]. The presence of limestone further promotes hemicarboaluminate and monocarboaluminate formation by providing $CaCO_3$ as a nucleation substrate [48, 55]. Together, these mechanisms explain the distinct hydration kinetics observed across T, TM, and TC systems.

LC^3 pastes exhibited less prominent endothermic peaks for CH, due to the pozzolanic reaction and dilution effect of the calcined-clay and limestone. The endothermic peaks for CH at 90 d were reduced or nearly equal to those at 7 d, due to the pozzolanic reactions that consumed and offset portlandite formed from clinker hydration. Correspondingly, the peak intensity for $CaCO_3$ decreased with the curing time due to its involvement in pozzolanic reaction to form the carbo-aluminates. The weight loss related to $CaCO_3$ peak went up in chemically activated clay samples due to the presence of zeolite minerals. Zeolites can adsorb CO_2 from the environment, when combined with $CaCO_3$, leading to continuous dissolution and formation of soluble calcium bicarbonate species. This resulted in weight loss as observed in the dTGA curve (**Fig. 12**). Overall, the TGA results agreed well with the test results of compressive strength, XRD, and pozzolanic reactivity.

Each activation method distinctly affected the properties of LC^3. Thermal activation improved the reactivity of clay via dehydroxylation. Mechanical activation enhanced the particle fineness and accelerated the consumption of portlandite. Chemical activation initiated early reactions of clay minerals, facilitating the gradual formation of AFt and AFm phases. Collectively, these mechanisms enhanced hydration kinetics, densified the microstructure, and improved the long-term performance of LC^3 samples [56]. These findings suggest that specifying thermal and mechanical activation yields the most durable LC^3 for aggressive environments, making them ideal choices for mix design focused on longevity and resilience.

3.2.3 Compressive strength

Fig. 13(a) and (b) present the effects of activation method and curing age on the compressive strength of OPC and LC^3-30 mortars. Overall, the performance of TM and TC activation techniques was inferior to T because of higher reactivity of thermally activated clays as verified in the reactivity tests (Sections 3.1.4 and 3.1.5), and they had a very similar effect on both the clays. LG underperformed compared to HG in all the activation scenarios. The compressive strength of M-HG-T was lower than M-OPC at 7 d, while it outperformed OPC at both 28 and 90 d. M-HG-TM and M-HG-TC specimens exhibited strengths comparable to M-OPC (within 90%) at 28 d and 90 d, as well as a slightly higher rate of strength gain from 28 d to 90 d, relative to M-OPC.

At 7 d, M-HG-T mortars had only 9% lower strength compared to M-OPC, while M-LG-T mortars had 20% lower strength. For M-TM, M-HG-TM and M-LG-TM specimens showed 18% and 24% lower strength compared to M-OPC, respectively. Thus, the difference between M-HG-TM and MLG-TM remained only 6%, which was 11% in T activated clays, suggesting that TM had a slightly better effect on improving the pozzolanic reactivity of low-grade clays. Also, the difference in strength of M-LG-T and M-LG-TM was only 3% while it was 10% in M-HG-T and M-HG-TM. For TC-based treatment, M-HG-TC exhibited 20% lower strength than M-OPC, while M-LG-TC again showed 24% lower strength than OPC. Thus, the influence of the activation methods of TM and TC had a slightly better effect on LG after 7 d of curing; compressive strength differed by 4-6% despite a significant difference in the kaolinite content of LG and HG.

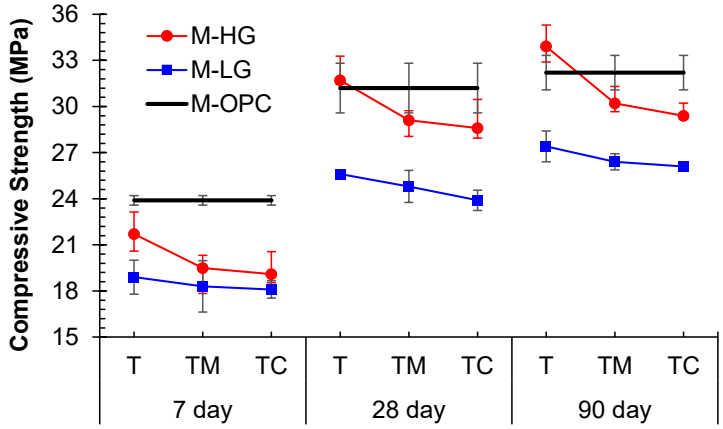

(a)

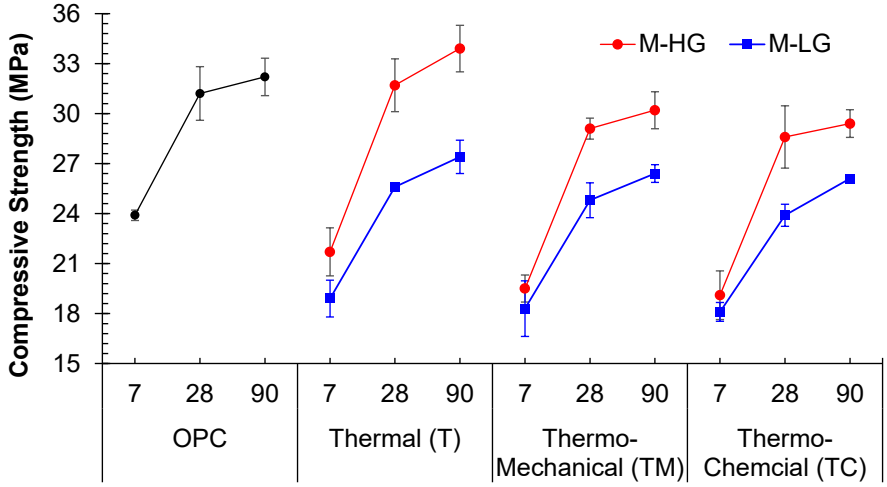

(b)

Fig. 13. Effects of (a) activation method and (b) curing age on the compressive strength of mortar.

The compressive strength of M-HG-T was 1.6% and 5% greater than that of control M-OPC at 28 d and 90 d, respectively, while the corresponding strength of M-LG-T was 17% and 14% lower than that of OPC. The delayed strength improvement in T-activated clays beyond 7 d, especially in HG, can be ascribed to: (1) the delayed nucleation of C-S-H and C-A-S-H gels, (2) the filler effect of

limestone, and (3) the delayed ettringite and carbo-aluminate formation. M-HG-TM and M-HG-TC exhibited about 6-8% lower strength than OPC for at 28 d and 90 d. On the other hand, M-LG-TM and M-LG-TC showed around 20-23% lower strength than control OPC at 28 d, while the corresponding strength difference after 90 d was reduced to 18-19%. The lower strength of M-LG in all cases was obvious due to its lower kaolinite content [57], while it showed improvement over age, especially in TM- and TC-activated clays.

Regarding the trends in strength development, the compressive strength of OPC was increased by 30.5% from 7 d to 28 d but only 3% further from 28 d to 90 d (**Fig. 13**(b)). The strength of M-HG-T increased 46.5% from 7 d to 28 d but only a further 6.9% from 28 d to 90 d, while M-LG-T had an intermediate (35.6%) increase in strength from 7 d to 28 d, but a 7% increase from 28 d to 90 d, respectively. Thus, the strength gain of both M-HG-T and M-LG-T was greater than M-OPC due to microstructure densification by the low-density phase formation with curing time in LC^3 [58]. For TM, the strength gain from 7 d to 28 d was 49.2 and 35.5% for M-HG-TM and M-LG-TM, respectively. From 28 d to 90 d, M-HG-TM and M-LG-TM showed further increase in strength by 3.8% and 6.5%, respectively. Thus, it can be noticed that TM imparted good strength gain in LG especially from 28 d onwards. This confirms the effectiveness of additional grinding on low-grade clays, which increased the surface area of calcined-clay particles, eventually improving their reactivity, when used in LC^3 [59].

In the case of TC treatment, the strength gain from 7 d to 28 d was 49.7% and 32% for M-HG-TC and M-LG-TC, respectively, and it was 2.8% and 9.2% for M-HG-TC and M-LG-TC, from 28 d to 90 d (**Fig. 13**(b)). The slower rate of strength gain in HG can be attributed to the reduced reactivity due to zeolite formation. However, it may prove advantageous for long-term durability prospects because zeolites have been proven to consume excess alkalis in cementitious systems, thus mitigating the risk of alkali-silica reaction [60, 61]. Zeolites can also act as ion exchangers, allowing for the selective removal of certain cations from pore solutions [53, 54], thereby potentially reducing the risk of deleterious chemical reactions [62]. Their adsorption properties enable the removal of contaminants, e.g., heavy metals or volatile organic compounds from water or air [63]. This makes zeolite-based blended cement systems particularly attractive for environmental sustainability. In the case of LG, the rate of strength gain was again greater for LG from 28 d to 90 d. TM and TC treatment methods showed strong potential particularly for LG, imparting slower but continued strength to 90 d. Thus, it is necessary to optimise treatment methods as per the mineralogy of clay to get the desired properties.

Fig. 14 illustrates a comparison of the compressive strength of mortar with LC^3-30 and LC^3-50. Recall that the LC^3-50 mixes (M-HG-T and M-LG-T) had only calcination (T) treatment, but at 50 ^oC higher temperatures than for the LC^3-30 mixes, which also underwent coupled mechanical or

chemical treatment. The LC^3-50 mixes also replaced 50% of OPC. The strength of LC^3-50 mortars was less than LC^3-30 mortars at all ages (7, 28 and 90 d), while the strength was nearly equal to LC^3-30 mortar mixes made with HG and with TM and TC activation. The lower strength at greater replacement of OPC at earlier stages was expected due to the reduction in the availability of calcium ions from cement, thus leading to the lesser formation of C-S-H gel [64]. Comparing the compressive strength of LG blends, the greater difference was observed between LC^3-50 (T) and LC^3-30 mixes made with TM and TC category. It was attributed to the better pozzolanic potential induced by the TM and TC activation techniques on LG as discussed earlier in **Fig. 13**. TM showed a stronger influence at 28 d due to increased surface area and hence reactive sites for the formation of hydration products [65]. The difference in strength between TM and TC was further reduced at 90 d in the case of M-LG. This again confirmed the potential of TM and TC for LG. The observed strength evolution reflected the following mechanisms: HG clays achieved improved strength due to a higher kaolinite content boosting pozzolanic reactivity; TM enhanced late-age performance of LG by increasing silica availability for reaction; TC activation led to limited reactivity because phase transformations reduced the amount of reactive phases.

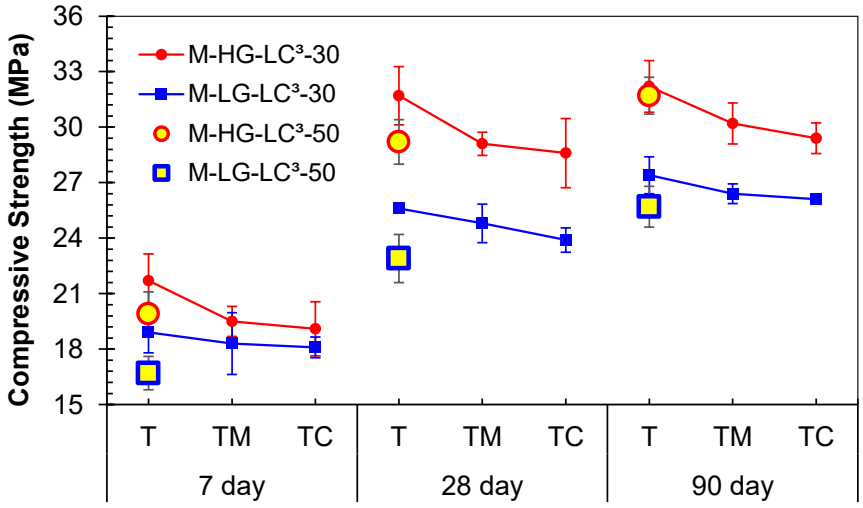

Fig. 14. Compressive strength of mortar comparing LC^3-30 and LC^3-50 with different activation methods.

4. Discussion

Thermal activation of clay induced dehydroxylation of kaolinite and illite, converting them into amorphous metakaolin phases with high pozzolanic reactivity [66]. XRD and TGA results confirmed the transformation of ordered aluminosilicate layers into a disordered structure with enhanced availability of reactive alumina and silica (**Table 3**). This was reflected in higher portlandite consumption and bound-water content, confirming greater reactivity (Fig. 7 and Fig. 8). TM further refined the particle size and disrupted crystalline phases, increasing surface area and enhancing early pozzolanic reactivity, particularly in low-grade clay [45, 46]. The TC route, involving alkali

treatment, introduced sodium ions into the clay lattice and partially converted dehydroxylated aluminosilicates into zeolite-like phases [35] also indicated in Fig. 5. The hydration reaction in paste, the strength evolution and correlation of reactivity with the strength has been explained in following sub-sections.

4.1 Hydration reactions and strength evolution

Upon blending with limestone and cement, the activated clays interacted with calcium hydroxide and carbonate ions to form secondary hydration products such as calcium aluminosilicate hydrates (C-A-S-H), ettringite, and carboaluminate phases [2, 3]. The high amorphous content in T-activated clays accelerated these reactions, increasing early hydration heat and phase formation as observed in XRD analyses (Section 3.1.2) and isothermal calorimetry (Section 3.1.3). TM activation enhanced the extent of these reactions by providing more nucleation sites and improving filler effects [48], while TC-activated clays exhibited slower reaction kinetics due to partial crystallinity from zeolitic phases [48]. The progressive consumption of portlandite and evolution of ettringite and monocarboaluminate phases in LC^3 systems confirm the synergistic role of limestone and activated clays in promoting stable, low-density hydrates that contribute to long-term strength and durability [67] .

The combined effects of activation on hydration kinetics and phase assemblage were evident in the strength-development trends (Section 3.2.4). LC^3 mortars containing thermally activated clays demonstrated superior compressive strength, surpassing OPC at later ages due to the dense microstructure produced by continued pozzolanic reactions [56]. TM activation particularly benefited the low-grade clay by enhancing later age strength, narrowing the performance gap between high and low grade clays (Fig. 14). The reduced but steady strength gain in TC-activated systems indicated the contribution of zeolitic phases to long-term stability and potential mitigation of detrimental reactions [62]. Overall, optimized thermal or thermo-mechanical activation promotes a balanced hydration process, rapid early reactivity coupled with sustained later age strength gain, while thermo-chemical activation may offer extended durability advantages [63].

4.2 Correlation and mechanistic interpretation

A strong link was observed between activation-induced structural changes and the hydration kinetics and mechanical performance of LC^3 systems. The degree of amorphization controlled reactive alumina and silica availability, governing secondary hydrate formation. Enhanced dissolution in T- and TM-activated clays accelerated pozzolanic reactions, promoting dense C-A-S-H and carboaluminate phases, pore refinement, and higher strength. In contrast, partial recrystallization in TC-activated clays delayed early reactions but ensured later-age stability. Overall, LC^3 performance was governed by the interaction between activation-induced disorder, hydrate evolution, and microstructural densification.

To further explain the relationship between hydration progress and mechanical performance, statistical correlations were developed among compressive strength (at 7, 28, and 90 d), bound water (BW) content, and the Modified Chapelle Test (MCT) values for HG and LG based LC^3. The correlation coefficients indicated a strong positive relationship between these parameters, as shown in **Fig. 15**. For HG-based LC^3 (**Fig. 15**a), strong correlations were observed between the Modified Chapelle Test (MCT) values and compressive strength at all curing ages (R = 0.93–0.94), confirming that higher intrinsic reactivity translated directly into greater strength gain. However, the bound water (BW) content exhibited only moderate correlation with MCT (R = 0.82) and relatively weak association with strength, indicating that in HG systems, where the thermal activation was already sufficient, the additional bound water formation did not proportionally affect strength at later ages.

In contrast, the LG-based LC^3 (**Fig. 15**b) exhibited consistently stronger and more coherent relationships among all parameters, with MCT–strength correlations above 0.95 and MCT–BW correlation exceeding 0.98. Notably, BW showed a much stronger association with later-age strength (28–90 d), suggesting that in low-grade systems, bound water was a more sensitive indicator of ongoing pozzolanic activity and microstructural densification. This implied that hydration and strength evolution in LG clays were more dependent on the progress of secondary pozzolanic reactions, which were governed by the activation process.

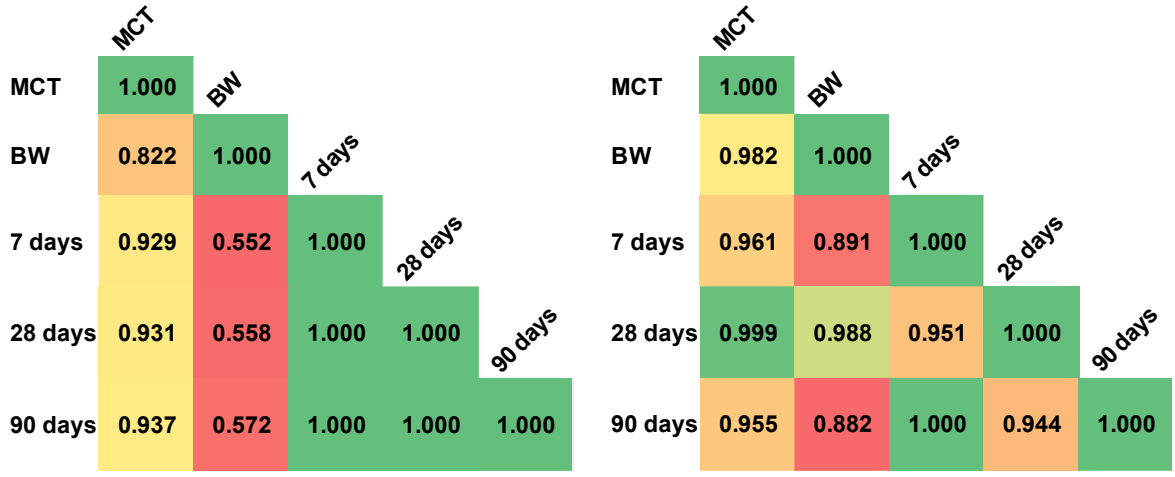

(a) HG based LC^3 (b) LG based LC^3

Fig. 15. Correlation matrix for reactivity and strength.

Fig. 16 illustrates the mechanistic interpretation of these activation routes, correlating microstructural evolution with strength development. In the T-activated clays, dehydroxylation breaks down the regular layered structure of clays, forming a disordered, amorphous aluminosilicate network. This structural disorder facilitates the rapid dissolution of silica and alumina, which drives high early-age strength gains. However, this rate diminishes as the reactive phases are consumed. The TM route intensifies this process; the combined action of heat and grinding further reduces particle

size, increases surface area, and disrupts any residual crystalline order. These changes provide more reactive surfaces, enhancing the formation of hydration products, particularly in low-grade clays, and supporting continued strength development at later ages. In contrast, TC activation introduces alkali ions that partially reorganize the dehydroxylated structure into zeolitic phases. While this can slightly reduce early reactivity in high-grade clays, it promotes a more stable matrix that improves long-term durability by binding alkalis and mitigating harmful reactions. The strength-gain trends in **Fig. 16** reflect these underlying mechanisms: extensive amorphization accelerates early strength, whereas controlled recrystallization promotes long-term stability.

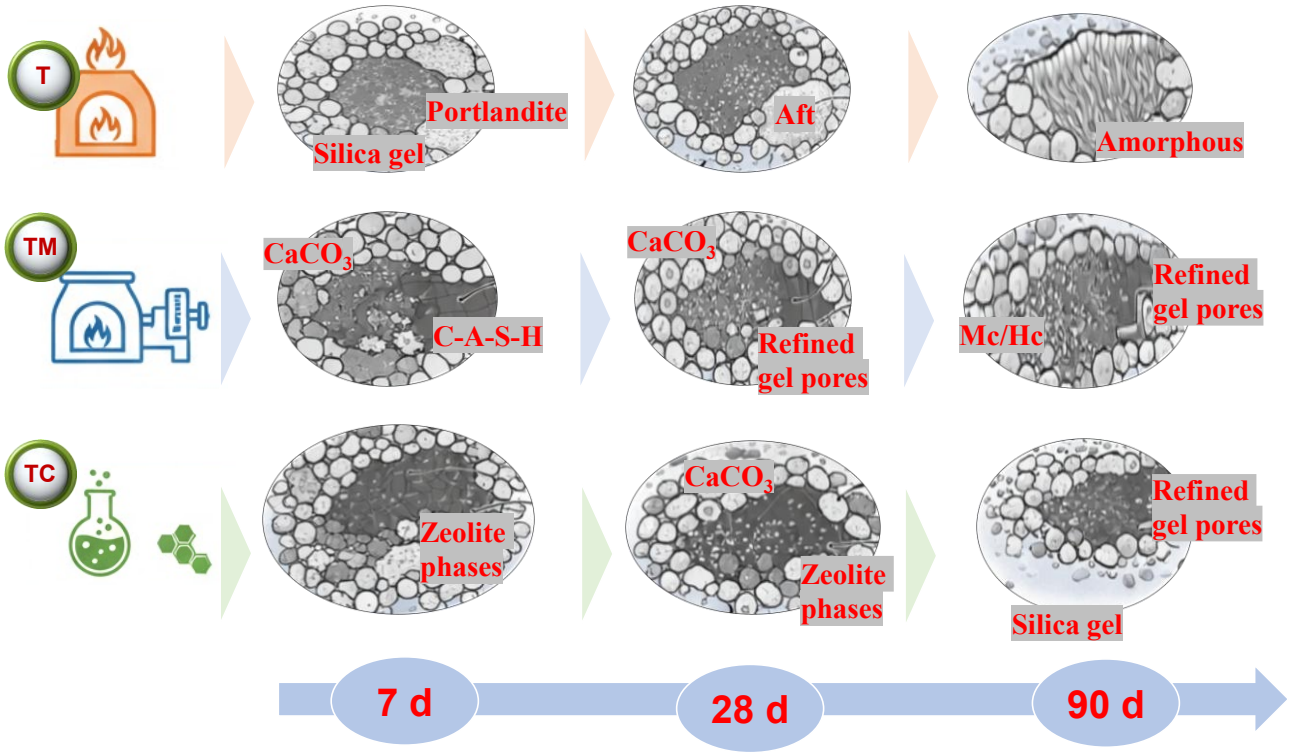

Fig. 16. Schematic illustration of underlying mechanisms affecting LC^3 strength.

5. Energy Analysis

5.1 Clay activation

A quantitative energy-balance analysis was conducted to evaluate the energy requirements of thermal (T), thermomechanical (TM), and thermochemical (TC) activation routes (**Table 4**), using industrial-scale data from DG Khan Cement Plant, Pakistan. In all activation routes, calcination represents the major fraction of total energy input [9, 68]. The calcination energy at 800 °C obtained from industry, is 374 kWh t^{-1}, which was adjusted linearly for the actual calcination temperatures used in this study. For the thermal route (T), HG clay was calcined at 750 °C, resulting in ≈351 kWh t^{-1}, and LG clay at 900 °C, requiring ≈421 kWh t^{-1}. These values represent the total energy consumption for pure thermal activation. For the thermomechanical route (TM), the calcination temperatures were reduced to 700 °C for HG and 850 °C for LG, lowering the calcination energy to ≈328 kWh t^{-1} (HG) and ≈398 kWh t^{-1} (LG). Additional mechanical activation using a raw mill

consumed 24.4 kWh t^{-1}. After accounting for industrial-scale optimization, the total energy requirement for TM was ≈350 kWh t^{-1} for HG and ≈ 410 kWh t^{-1} for LG, demonstrating that TM activation provides modest energy savings relative to full thermal activation while significantly enhancing the surface area and pozzolanic reactivity of low-grade clays. For the thermochemical route (TC), standard calcination at the reduced temperatures (HG: 700 °C, LG: 850 °C) was combined with chemical activation, including NaOH treatment, oven drying, centrifugation, and vacuum filtration (~35 kWh t^{-1}). This results in a total energy consumption of ≈363 kWh t^{-1} for HG and ≈433 kWh t^{-1} for LG, making TC the most energy-intensive route despite its potential benefits for long-term durability. In summary, the energy-balance analysis demonstrates that calcination dominates energy consumption, TM activation is the most energy-efficient strategy due to reduced calcination and minimal milling energy, and TC activation requires the highest energy input due to additional chemical processing. This quantitative evaluation provides a logical and industrially relevant basis for selecting TM as a sustainable activation method for enhancing the reactivity of low-grade clays in LC^3 production.

Table 4 Energy consumption of various clay activation treatments.

Activation route	Calcination temperature (°C)		Energy consumption (kWh t^{-1})	
	HG clay	LG clay	HG clay	LG clay
Thermal (T)	750	900	351	421
Thermomechanical (TM)	700	850	350	410
Thermochemical (TC)	700	850	363	433

5.2 Cement manufacturing

Afterwards, energy calculations were done for OPC and LC^3 prepared with three types of activated clays. The energy values corresponding to each activity in OPC production are presented in **Table 5**. While LC^3 calculations are based on similar activities except for clay activation energy which is calculated prior and presented in **Table 4**. Calculations are done based on the material composition presented in Section 2.3. Carbon emission values were also taken corresponding to each activity and are presented in **Table 5**. Following this procedure, the total energy consumption and CO_2 emissions of OPC and LC^3 prepared with T, TM and TC are presented in **Table 6**. Energy consumption of LC^3 variants reduced by 22 – 24 % in comparison to OPC, with TM giving the least energy consumption. CO_2 emissions reduced by 20-24% in comparison to OPC with T and TM representing nearly same emissions while TC showed slightly higher CO_2 emissions.

Table 5 Energy consumption and CO_2 emissions of various activities in production of OPC.

Activity	OPC energy (kWh/ton)	Emission factor
Quarry	1.7	2.45 kg CO_2/L

Transport	5.1	2.45 kg CO_2/L
Fuel	784.4	0.30 t CO_2/ton
Crusher	1.4	0.61 t CO_2/MWh
Raw mill	24.5	0.61 t CO_2/MWh
Calcination	875.0	0.60 t CO_2/ton
Kiln+Cooler+Coal mill	27.0	0.0788 t CO_2/GJ
Cement mill	30.0	0.61 t CO_2/MWh
Logistics (avg. 200 km)	30.3	

Table 6 Energy consumption and CO_2 emissions of OPC versus LC^3.

Cement type	Energy consumption (kWh/ton)	CO_2 emissions (ton/ton of cement)
OPC	1779	0.82
LC^3-T	1351	0.63
LC^3-TM	1348	0.64
LC^3-TC	1354	0.65

6. Conclusions

This study evaluated the influences of thermal (T), thermo-mechanical (TM), and thermo-chemical (TC) activation methods on high-grade (HG) and low-grade (LG) kaolinitic clays for their applications in LC^3 systems. The main conclusions can be drawn as follows:

1) Thermal (T) and thermo-mechanical (TM) activation effectively dehydroxylated kaolinite and illite, increasing amorphous content and reactive alumina/silica, whereas thermo-chemical (TC) activation reduced SiO_2 by up to 26% in HG clay, incorporated 12% Na_2O, and formed stable zeolitic phases, limiting early reactivity.
2) Reactivity tests confirmed T-activated HG clays consumed 1174 mg/g $Ca(OH)_2$ in the modified Chapelle test, while LG clays reached 880 mg/g; TM activation increased bound water to over 8% in HG and enhanced hydration in LG, whereas TC activation had lower reactivity. The correlation between Modified Chapelle Test (MCT) values and compressive strength was very high (R = 0.93–0.95).
3) LC^3 mortars with T-activated HG clays achieved compressive strengths of 1.6% and 5% higher than OPC at 28 and 90 d, respectively; M-LG-T mortars were 17% and 14% lower than OPC. TM and TC activation improved later-age strength in LG, with strength gain from 28 to 90 d reaching 6.5–9.2%. Cumulative hydration heat was highest for M-HG-T, followed by TM, and lowest for TC-activated clays.
4) LC^3-50 mortars replacing 50% OPC showed lower early-age strength than LC^3-30, but TM and TC activation improved LG mortars at 28 d (strength increase ~35–36%) and 90 d

(strength increase 6–9%), indicating the effectiveness of mechanical and chemical activation for low-grade clays.

5) Optimising activation according to clay type is critical: T activation is ideal for high-kaolinite clays, TM enhances low-kaolinite clay reactivity, and TC may offer potential for long-term durability through stable zeolite formation.

7. Limitations

Although this study provides important insights into the thermo-mechanical and thermo-chemical activation of low- and high-grade clays for LC^3 production, several limitations must be acknowledged.

1) The mineralogical variability of natural clays may be broader than the two representative samples used here, and clays with different impurity levels or mixed-layer structures may respond differently to the activation routes.
2) The calcination, grinding, and chemical treatment conditions were implemented under controlled laboratory settings, which may not fully reflect industrial-scale heat transfer efficiency, residence-time fluctuations, or mechanical energy losses.
3) The thermo-chemical activation route was assessed using a single alkali concentration and treatment duration; thus, the broader optimisation space was not explored.
4) The hydration, reactivity, and strength evolution were evaluated only up to 90 d, and long-term durability parameters such as chloride penetration, carbonation resistance, and alkali silica reaction mitigation were not investigated.
5) Finally, the energy assessment relies on energy-intensity values obtained from a single industrial cement plant, which may not capture regional or technological variability across different production facilities. These limitations highlight the need for future work to expand the range of clay sources, optimise activation parameters, evaluate long-term durability, and validate energy performance across multiple industrial settings.

Acknowledgements

Authors are thankful to the Fluxx Grant #G-2506-802320637 / Grant # 25-3398’ from ClimateWorks Foundation, USA awarded to NED University of Engineering & Technology, Karachi for NC4SCM, and D.G. Cement for initiating centre for low-carbon construction materials in Department of Architectural Engineering and Design, University of Engineering & Technology, Lahore, Pakistan

References

[1] S. Krishnan, S.K. Kanaujia, S. Mithia, S. Bishnoi, Hydration kinetics and mechanisms of carbonates from stone wastes in ternary blends with calcined clay, Construction and Building Materials 164 (2018) 265-274.

[2] K. Scrivener, F. Martirena, S. Bishnoi, S. Maity, Calcined clay limestone cements (LC3), Cement and Concrete Research 114 (2018) 49-56.

[3] B. Luzu, R. Trauchessec, A. Lecomte, Packing density of limestone calcined clay binder, Powder Technology 408 (2022) 117702.

[4] M. Fatima, M. Ltifi, K. Rashid, I. Zafar, Clay Mineralogy and its Role in Advancing Limestone Calcined Clay Cement (LC3): A Comprehensive Review with Scientometric Analysis, Advanced Concrete Technology 23 (2026) 596-611.

[5] N. Blouch, K. Rashid, I. Zafar, M. Ltifi, M. Ju, Prioritization of low-grade kaolinite and mixed clays for performance evaluation of Limestone Calcined Clay Cement (LC3): Multi-criteria assessment, Applied Clay Science 243 (2023) 107080.

[6] R. San Nicolas, T. Wang, M. Rupasinghe, Effect of calcined clays from Victoria, Australia as cement substitution in ternary blended cement systems, Case Studies in Construction Materials 20 (2024).

[7] V.A. Baki, X. Ke, A. Heath, J. Calabria-Holley, C. Terzi, M. Sirin, The impact of mechanochemical activation on the physicochemical properties and pozzolanic reactivity of kaolinite, muscovite and montmorillonite, Cement and Concrete Research 162 (2022) 106962.

[8] M. Fatima, K. Rashid, M. Ahmad, M. Ju, S.M. Saleem Kazmi, M.J. Munir, Development and comparative assessment of low-carbon LC3 and geopolymer blocks through pressure casting, Journal of Building Engineering 104 (2025) 112379.

[9] M. Fatima, M. Ltifi, K. Rashid, I. Zafar, Clay activation through CO2-derived oxalic acid for advancing its reactivity and strength of limestone calcined clay cement (LC3), Case Studies in Construction Materials 24 (2026) e05684.

[10] M. Fatima, M. Ltifi, K. Rashid, I. Zafar, Acidic and Alkaline Activation Routes for Enhancing Low-Grade Clays Performance in Developing Limestone Calcined Clay Cement LC3 Innovative Infrastructure Solutions (2026).

[11] P. Komadel, Chemically modified smectites, Clay Minerals 38(1) (2003) 127-138.

[12] I.B. Borno, N. Nair, W. Ashraf, Alkali thermal fusion: A prospective route to enhance the reactivity of low-grade clay and utilize as supplementary cementitious material (SCM), Cement and Concrete Composites 147 (2024).

[13] I.B. Borno, W. Ashraf, Insights into the role of calcination temperature and NaOH dosage in producing supplementary cementitious materials from low-grade clay via alkali-thermal-fusion, Applied Clay Science 258 (2024).

[14] C. Belver, M.A. Bañares Muñoz, M.A. Vicente, Chemical activation of a kaolinite under acid and alkaline conditions, Chemistry of materials 14(5) (2002) 2033-2043.

[15] K. Okada, Y. Kameshima, A. Yasumori, Chemical shifts of silicon X-ray photoelectron spectra by polymerization structures of silicates, Journal of the American Ceramic Society 81(7) (1998) 1970-1972.

[16] B. Ayati, D. Newport, H. Wong, C. Cheeseman, Acid activated smectite clay as pozzolanic supplementary cementitious material, Cement and Concrete Research 162 (2022) 106969.

[17] M. Pentrák, V. Hronský, H. Pálková, P. Uhlík, P. Komadel, J. Madejová, Alteration of fine fraction of bentonite from Kopernica (Slovakia) under acid treatment: A combined XRD, FTIR, MAS NMR and AES study, Applied Clay Science 163 (2018) 204-213.

[18] R. Snellings, Assessing, Understanding and Unlocking Supplementary Cementitious Materials, Rilem Technical Letters 1 (2016) 50-55.

[19] S. Donatello, M. Tyrer, C. Cheeseman, Comparison of test methods to assess pozzolanic activity, Cement and Concrete Composites 32(2) (2010) 121-127.

[20] A. Parashar, S. Bishnoi, A comparison of test methods to assess the strength potential of plain and blended supplementary cementitious materials, Construction and Building Materials 256 (2020) 119292.

[21] A. Tironi, M.A. Trezza, A.N. Scian, E.F. Irassar, Assessment of pozzolanic activity of different calcined clays, Cement and concrete composites 37 (2013) 319-327.

[22] F. Avet, R. Snellings, A.A. Diaz, M.B. Haha, K. Scrivener, Development of a new rapid, relevant and reliable (R3) test method to evaluate the pozzolanic reactivity of calcined kaolinitic clays, Cement and Concrete Research 85 (2016) 1-11.

[23] X. Li, e.a. Snellings, Reactivity tests for supplementary cementitious materials: RILEM TC 267-TRM phase 1, Materials and Structures 51 (2018) 1-14.

[24] X. Li, R. Snellings, M. Antoni, N.M. Alderete, M. Ben Haha, S. Bishnoi, Ö. Cizer, M. Cyr, K. De Weerdt, Y. Dhandapani, J. Duchesne, J. Haufe, D. Hooton, M. Juenger, S. Kamali-Bernard, S. Kramar, M. Marroccoli, A.M. Joseph, A. Parashar, C. Patapy, J.L. Provis, S. Sabio, M. Santhanam, L. Steger, T. Sui, A. Telesca, A. Vollpracht, F. Vargas, B. Walkley, F. Winnefeld, G. Ye, M. Zajac, S. Zhang, K.L. Scrivener, Reactivity tests for supplementary cementitious materials: RILEM TC 267-TRM phase 1, Materials and Structures 51(6) (2018) 151.

[25] F. Avet, K. Scrivener, Simple and reliable quantification of kaolinite in clay using an oven and a balance, Calcined Clays for Sustainable Concrete: Proceedings of the 3rd International Conference on Calcined Clays for Sustainable Concrete, Springer, 2020, pp. 147-156.

[26] F. Zunino, K. Scrivener, Reactivity of kaolinitic clays calcined in the 650 °C–1050 °C temperature range: Towards a robust assessment of overcalcination, Cement and Concrete Composites 146 (2024).

[27] S.A. Bernal, M.C.G. Juenger, X. Ke, W. Matthes, B. Lothenbach, N. De Belie, J.L. Provis, Characterization of supplementary cementitious materials by thermal analysis, Materials and Structures 50(1) (2016) 26.

[28] A. C109, ASTM C109/C109M, Standard Test Method for Compressive Strength of Hydraulic Cement Mortars (Using 2-in. or 50-mm Cube Specimens), ASTM International, West Conshohocken PA, 2008.

[29] T. Hanein, K.-C. Thienel, F. Zunino, A.T. Marsh, M. Maier, B. Wang, M. Canut, M.C. Juenger, M. Ben Haha, F. Avet, Clay calcination technology: state-of-the-art review by the RILEM TC 282-CCL, Materials and Structures 55(1) (2022) 3.

[30] A. Sedaghat, A. Zayed, P.J.J.o.T. Sandberg, Evaluation, Measurement and Prediction of Heat of Hydration of Portland Cement Using Isothermal Conduction Calorimetry, 41(6) (2013) 943-950.

[31] V.A. Drits, A. Derkowski, Kinetic behavior of partially dehydroxylated kaolinite, American Mineralogist 100(4) (2015) 883-896.

[32] E. Gasparini, S.C. Tarantino, P. Ghigna, M.P. Riccardi, E.I. Cedillo-González, C. Siligardi, M. Zema, Thermal dehydroxylation of kaolinite under isothermal conditions, Applied Clay Science 80 (2013) 417-425.

[33] R. Dewi, H. Agusnar, Z. Alfian, Tamrin, Characterization of technical kaolin using XRF, SEM, XRD, FTIR and its potentials as industrial raw materials, Journal of Physics: Conference Series, IOP Publishing, 2018, p. 042010.

[34] A. Kumar, P. Lingfa, Sodium bentonite and kaolin clays: Comparative study on their FT-IR, XRF, and XRD, Materials Today: Proceedings 22 (2020) 737-742.

[35] Y. Liu, S. Han, D. Guan, S. Chen, Y. Wu, Y. Yang, N. Jiang, Rapid green synthesis of ZSM-5 zeolite from leached illite clay, Microporous and Mesoporous Materials 280 (2019) 324-330.

[36] R. Fernandez, F. Martirena, K.L. Scrivener, The origin of the pozzolanic activity of calcined clay minerals: A comparison between kaolinite, illite and montmorillonite, Cement and Concrete Research 41(1) (2011) 113-122.

[37] S. Hollanders, R. Adriaens, J. Skibsted, Ö. Cizer, J. Elsen, Pozzolanic reactivity of pure calcined clays, Applied Clay Science 132 (2016) 552-560.

[38] G. Christidis, P. Makri, V. Perdikatsis, Influence of grinding on the structure and colour properties of talc, bentonite and calcite white fillers, Clay Minerals 39(2) (2004) 163-175.

[39] C. He, Thermal stability and pozzolanic activity of raw and calcined mixed-layer micarsmectite, Applied Clay Science 17 2000 141–161 17(3-4) (2000) 141-161.

[40] J.L. Provis, J.S.J. van Deventer, Geopolymerisation kinetics. 1. In situ energy-dispersive X-ray diffractometry, Chemical Engineering Science 62(9) (2007) 2309-2317.

[41] Z. Zhang, H. Wang, J.L. Provis, F. Bullen, A. Reid, Y. Zhu, Quantitative kinetic and structural analysis of geopolymers. Part 1. The activation of metakaolin with sodium hydroxide, Thermochimica Acta 539 (2012) 23-33.

[42] M.U. Rehman, A.J. MacLeod, W.P. Gates, Phase development and mechanical strength of limestone calcined clay cement utilising Australian bentonite and plasterboard waste, Construction and Building Materials 445 (2024) 137937.

[43] K. Scrivener, F. Avet, H. Maraghechi, F. Zunino, J. Ston, W. Hanpongpun, A. Favier, Impacting factors and properties of limestone calcined clay cements (LC3), Green Materials 7(1) (2019) 3-14.

[44] M. Slaný, E. Kuzielová, M. Žemlička, M. Matejdes, A. Struhárová, M.T. Palou, Metabentonite and metakaolin-based geopolymers/zeolites: relation between kind of clay, calcination temperature and concentration of alkaline activator, Journal of Thermal Analysis and Calorimetry 148(20) (2023) 10531-10547.

[45] V.V. Boldyrev, Mechanochemistry and mechanical activation of solids, Russian chemical reviews 75(3) (2006) 177.

[46] E. Kristof, A.Z. Juhasz, I. Vassanyi, The effect of mechanical treatment on the crystal structure and thermal behavior of kaolinite, Clays and Clay Minerals 41 (1993) 608-612.

[47] É. Makó, R.L. Frost, J. Kristóf, E. Horváth, The Effect of Quartz Content on the Mechanochemical Activation of Kaolinite, Journal of Colloid and Interface Science 244(2) (2001) 359-364.

[48] A.H. Ahmed, S. Nune, M. Liebscher, T. Köberle, A. Willomitzer, I. Noack, M. Butler, V. Mechtcherine, Exploring the role of dilutive effects on microstructural development and hydration kinetics of limestone calcined clay cement (LC3) made of low-grade raw materials, Journal of Cleaner Production (2023) 139438.

[49] R. Hay, L. Li, K. Celik, Shrinkage, hydration, and strength development of limestone calcined clay cement (LC3) with different sulfation levels, Cement and Concrete Composites 127 (2022) 104403.

[50] A. Huraira, M. Ltifi, K. Rashid, I. Zafar, Boosting early strength in limestone calcined clay cement (LC3) and its phase evolution using waste-derived silica mineral, Case Studies in Construction Materials 23 (2025) e05484.

[51] L.G. Baquerizo, T. Matschei, K.L. Scrivener, Impact of water activity on the stability of ettringite, Cement and Concrete Research 79 (2016) 31-44.

[52] J. Csizmadia, G. Balázs, F.D. Tamás, Chloride ion binding capacity of aluminoferrites, Cement and Concrete Research 31(4) (2001) 577-588.

[53] A. Dyer, Ion-exchange properties of zeolites, Studies in Surface Science and Catalysis 157 (2005) 181-204.

[54] A. Dyer, Ion-exchange properties of zeolites and related materials, Studies in surface science and catalysis (2007) 525-553.

[55] F. Zunino, K. Scrivener, Microstructural developments of limestone calcined clay cement (LC3) pastes after long-term (3 years) hydration, Cement and Concrete Research 153 (2022) 106693.

[56] J. Mañosa, A. Maldonado-Alameda, J.M. Chimenos, Mechanical activation of muscovite-rich clay: A novel approach for ternary blended cement, Construction and Building Materials 489 (2025) 142182.

[57] F. Zunino, K.L. Scrivener, Improving the Behaviour of Calcined Clay as Supplementary Cementitious Materials by a Combination of Controlled Grinding and Particle Selection, in: S. Bishnoi (Ed.) Calcined Clays for Sustainable Concrete, Springer Singapore, Singapore, 2020, pp. 157-162.

[58] Y. Dhandapani, T. Sakthivel, M. Santhanam, R. Gettu, R.G. Pillai, Mechanical properties and durability performance of concretes with Limestone Calcined Clay Cement (LC3), Cement and Concrete Research 107 (2018) 136-151.

[59] A. Souri, H. Kazemi-Kamyab, R. Snellings, R. Naghizadeh, F. Golestani-Fard, K. Scrivener, Pozzolanic activity of mechanochemically and thermally activated kaolins in cement, Cement and Concrete Research 77 (2015) 47-59.

[60] M.S. Islam, B.J. Mohr, Effect of treated clinoptilolite zeolite on alkali-silica reaction, Materials Today: Proceedings (2023).

[61] A. Zolghadri, B. Ahmadi, H. Taherkhani, Influence of natural zeolite on fresh properties, compressive strength, flexural strength, abrasion resistance, Cantabro-loss and microstructure of self-consolidating concrete, Construction and Building Materials 334 (2022) 127440.

[62] F. Naiqian, M. Changchen, J. Xihuang, Natural zeolite for preventing expansion due to alkali-aggregate reaction, Cement, Concrete and Aggregates 14(2) (1992).

[63] Y. Tao, H. Kanoh, L. Abrams, K. Kaneko, Mesopore-modified zeolites: preparation, characterization, and applications, Chemical reviews 106(3) (2006) 896-910.

[64] M. Sharma, S. Bishnoi, F. Martirena, K. Scrivener, Limestone calcined clay cement and concrete: A state-of-the-art review, Cement and Concrete Research 149 (2021) 106564 %@ 0008-8846.

[65] S. Barbhuiya, J. Nepal, B.B. Das, Properties, compatibility, environmental benefits and future directions of limestone calcined clay cement (LC3) concrete: A review, Journal of Building Engineering (2023) 107794 %@ 2352-7102.

[66] F. Avet, E. Boehm-Courjault, K. Scrivener, Investigation of C-A-S-H composition, morphology and density in Limestone Calcined Clay Cement (LC3), Cement and Concrete Research 115 (2019) 70-79.

[67] S. Krishnan, A.C. Emmanuel, S. Bishnoi, Hydration and phase assemblage of ternary cements with calcined clay and limestone, Construction and Building Materials 222 (2019) 64-72.

[68] K. Rashid, M. Ltifi, I. Zafar, M. Ju, Performance enhancement of limestone calcined clay cement (LC3) using shale: industrial implementation Perspectives, Engineering Science and Technology, an International Journal 69 (2025) 102106.